

## 激光/等离子定向能量沉积 316L 不锈钢成型尺寸及力学性能的对比

秦文韬, 杨永强\*, 翁昌威, 韩昌骏

华南理工大学机械与汽车工程学院, 广东 广州 510640

**摘要** 作为当前最热门的增材制造技术之一,定向能量沉积可以实现大尺寸零件的高效成型。激光和电弧是定向能量沉积系统中最常用的热源,但它们在能量输入、能量分布以及与材料的作用机制等方面都存在差异。为此,本文对比了激光和等离子定向能量沉积 316L 不锈钢单道和薄壁件在尺寸、显微组织、力学性能方面的差异,以揭示两种工艺成型零件的差异。结果表明,在所选的工艺窗口内,激光在冷基板上沉积首层的结合效果要好于等离子。等离子定向能量沉积和激光定向能量沉积的工艺参数对单道尺寸的影响程度不同:在等离子定向能量沉积过程中,电流对层宽的影响最大,然后依次为送粉量和扫描速度,送粉量对层高的影响最大,之后依次是电流和扫描速度;在激光定向能量沉积过程中,扫描速度对层宽的影响最大,然后依次是送粉量和激光功率,送粉量对层高的影响最大,之后依次为扫描速度和激光功率。拉伸试验和显微硬度的测试结果表明:等离子定向能量沉积样件与激光定向能量沉积样件的力学性能相近,激光成型试样的抗拉强度可达 593 MPa,等离子成型试样的抗拉强度可达 570 MPa;但两者的显微组织存在较大差别,等离子成型试样中以定向生长的细长柱状晶为主,而激光成型试样中的柱状晶较短,不同区域的柱状晶生长方向各异。

**关键词** 激光技术;定向能量沉积;激光增材制造;等离子弧增材制造;316L 不锈钢

**中图分类号** TN249;TG444

**文献标志码** A

**doi:** 10.3788/CJL202148.2202006

### 1 引言

定向能量沉积是一种采用高能束将材料同步熔化沉积的增材制造工艺,该工艺通过机械装置控制沉积装置移动来达到材料沉积成型的目的<sup>[1]</sup>。常用的高能束源有激光、电子束以及电弧<sup>[2-3]</sup>。目前,基于激光的定向能量沉积系统已较为成熟。早在 1997 年,美国 Optomec 公司就推出了商业化的“LENS 750”设备<sup>[4]</sup>。等离子弧是一种压缩电弧,与自由电弧相比,其稳定性更好,能量也更集中。与激光选区熔化技术相比,定向能量沉积效率更高,适合大尺寸构件的制造。

在激光定向能量沉积方面,Sciammarella 等<sup>[5]</sup>研究了激光定向能量沉积过程中功率、移动速度、送粉量等参数的变化对 316L 不锈钢显微组织、力学性能的影响,并发现通过保持送粉量与移动速度之

比及单位距离内的净热输入不变,可获得均匀细小的胞状晶,成型件的显微硬度高于 227 HV。该研究结果可用于不同定向能量沉积设备的工艺校准。Yadollahi 等<sup>[6]</sup>研究了沉积层之间的时间间隔和热处理对成型件显微组织、力学性能的影响,结果发现:延长层间沉积间隔会使激光穿透深度降低,层间的冶金结合变得薄弱,孔隙率有所增加,获得的成型件的组织更细小、强度更高,但延伸率有所下降;均质化退火会使各区域的显微组织变得一致,晶粒尺寸有所增大,成型件的强度有所降低,但延伸率得以提高。Saboori 等<sup>[7]</sup>研究了沉积路径对 316L 不锈钢力学性能和残余应力的影响,并发现:与层间旋转 90°成型试样相比,层间旋转 67°成型试样的冷却速率更小,抗拉强度和延伸率分别降低 7%和 27%;与层间旋转 67°成型立方体相比,层间旋转 90°成型立方体侧面的残

收稿日期:2021-04-06;修回日期:2021-05-14;录用日期:2021-06-02

基金项目:广东省重点研发计划(2018B090905001)、国家自然科学基金(U2001218,51875215,81772428)、广东省特支计划(2019TQ05Z110)、广东省区域联合基金重点项目(2020B1515120013)

通信作者:\*meyqyang@scut.edu.cn

余应力更高,但两者顶面的残余应力较为接近。

在电弧定向能量沉积方面,Chen 等<sup>[8]</sup>采用熔化极气体保护电弧技术成型了 316L 不锈钢,其显微组织由不同形态的  $\delta$  相、 $\gamma$  相和  $\sigma$  相组成, $\sigma$  相的存在提高了 316L 不锈钢试样的显微硬度和抗拉强度,但  $\sigma$  相内产生的微裂纹逐渐发展成为大裂纹,并最终导致了试样的断裂。王凯博等<sup>[9]</sup>使用脉冲等离子弧技术打印了 IN738LC 单道,并发现在相同的热输入条件下,可以通过调整占空比和峰值电流来控制组织在柱状晶与等轴晶之间转变。

定向能量沉积过程中的热输入和热输入历史是影响组织和性能的主要因素。激光具有较高的能量密度和较小的热影响区,因此激光定向能量沉积成型的零件性能更高,而且激光的光斑尺寸也易于调整,但激光器及激光熔覆装置的价格较高;等离子定向能量沉积系统的设备成本比较低且沉积效率较高,但其成型精度较低。这两种热源在能量密度以及与材料的相互作用机制上存在差异,因此可能会对成型件的组织、性能造成影响。鉴于此,本文从单道成型件及单道多层构建的薄壁件的尺寸、组织、性能等方面对这两种定向能量沉积工艺进行了对比。

## 2 试验设备及研究方法

### 2.1 试验设备

本试验采用的定向能量沉积设备为实验室自行搭建的一套基于机器人平台的激光/等离子复合增减材制造系统,该系统由 PLC 控制柜、机械臂及其附加轴、等离子电源、激光器、水冷循环系统及机器人运动控制器组成,如图 1 所示。该系统采用双机



图 1 定向能量沉积设备实物图

Fig. 1 Appearance of directed energy deposition system

器人方案,系统灵活度高,成型范围大,可同时安装激光增材模块和等离子增材模块,结合了激光成型性能高和等离子弧成型效率高的优点。该系统可以同时安装增材模块及铣削减材模块,可以交替进行增减材工序,实现高性能复杂零件的高精度加工。

激光增材模块配备有 6000 W 多模连续光纤激光器,成型平面上的光斑直径约为 3 mm,三孔式喷嘴与成型平面之间的距离为 15 mm。等离子增材模块配备 TA-1 型焊枪,其喷嘴孔径为 2.5 mm,工作电流为 1~80 A,钨针内缩量为 2 mm。外部设备的输入输出全部连接至 PLC 控制柜,再由 Profinet 总线与机器人控制柜通信。机器人的运动控制及外部设备控制由 Rapid 语言编程实现,将 Rapid 代码导入机器人示教器内运行即可。

### 2.2 试验材料

本试验中选用的粉末为 316L 不锈钢粉末,粉末粒径范围为 60~125  $\mu\text{m}$ ,具体化学成分如表 1 所示,形貌如图 2 所示。基体材料同样为 316L 不锈钢,尺

表 1 316L 不锈钢粉末的化学成分

Table 1 Chemical composition of 316L stainless steel powder

Element	Si	Cr	Ni	Mn	Mo	C	O	Fe
Mass fraction /%	0.59	17.3	12.23	1.22	2.17	0.013	0.029	Bal.

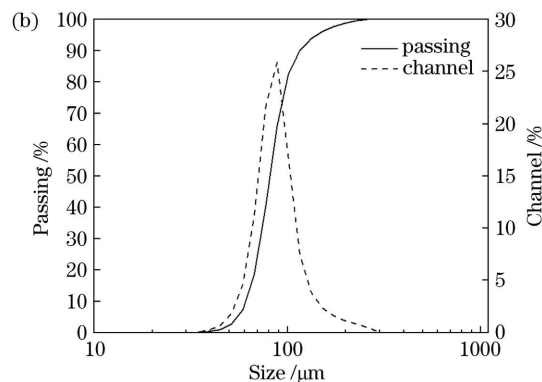
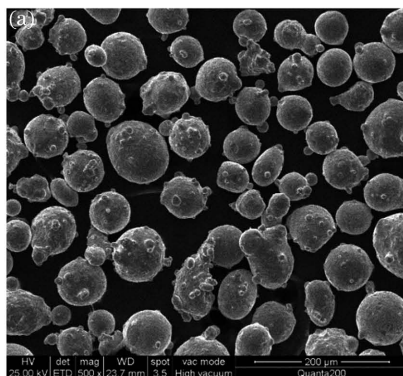


图 2 316L 不锈钢粉末的特征。(a)SEM 图;(b)粉末粒径分布

Fig. 2 Characteristic of 316L stainless steel powder. (a) SEM image; (b) particle size distribution

寸为 200 mm×100 mm×10 mm。成型前,基板均经过砂纸打磨及酒精清洗,以去除基板表面的氧化物。

### 2.3 试验方法

为对比两种工艺单道成型的差异,分别采用两种工艺沉积了长度为 80 mm 的单道;然后根据沉积前后基板质量的变化计算消耗的粉末质量,根据送粉速率及加工时间计算沉积质量,从而得出两种工艺的粉末利用率。在单道中段取样,采用盐酸+氯

化铁溶液对试样进行浅腐蚀,观察截面形貌。

为建立定向能量沉积尺寸的预测模型,设计了二次正交旋转试验,并结合实验室此前在等离子定向能量沉积方面的工作,对比两种工艺下工艺参数对尺寸影响的异同。表 2 为激光定向能量沉积的二次正交旋转组合试验因素水平表。每一组参数打印 10 层薄壁件,打印完成后在中部稳定区域取三处位置,测量平均层宽和层厚。

表 2 激光定向能量沉积的二次正交旋转组合试验因素水平表

Table 2 Factors and levels of quadratic orthogonal rotation combination test in laser directed energy deposition

Factor level	Laser power /W	Scanning speed /( $\text{mm}\cdot\text{min}^{-1}$ )	Powder feed rate /( $\text{g}\cdot\text{min}^{-1}$ )
-1.68179	1659	278	10.9
-1	2000	360	15
0	2500	480	21
1	3000	600	27
1.68179	3341	682	31.1

分别采用激光和等离子弧两种热源成型了 80 mm×3 mm×100 mm 的薄壁件,试验用工艺参数如表 3 所示,这些参数分别位于高功率激光定向能量沉积和微束等离子弧定向能量沉积的工艺区

间<sup>[10-11]</sup>。两组样品具有相近的粉末沉积密度及单位距离输入能量。分别在垂直方向、斜 45°方向和水平方向上制取拉伸试样。图 3 为拉伸试样的取样方向及尺寸参数示意图。

表 3 薄壁件的成型工艺参数

Table 3 Processing parameters used in directed energy deposition of thin-wall parts

Heat source	Laser power /W	Current /A	Scanning speed /( $\text{mm}\cdot\text{s}^{-1}$ )	Powder feed rate /( $\text{g}\cdot\text{min}^{-1}$ )
Laser	2000		10	24
Plasma arc		30	5	12

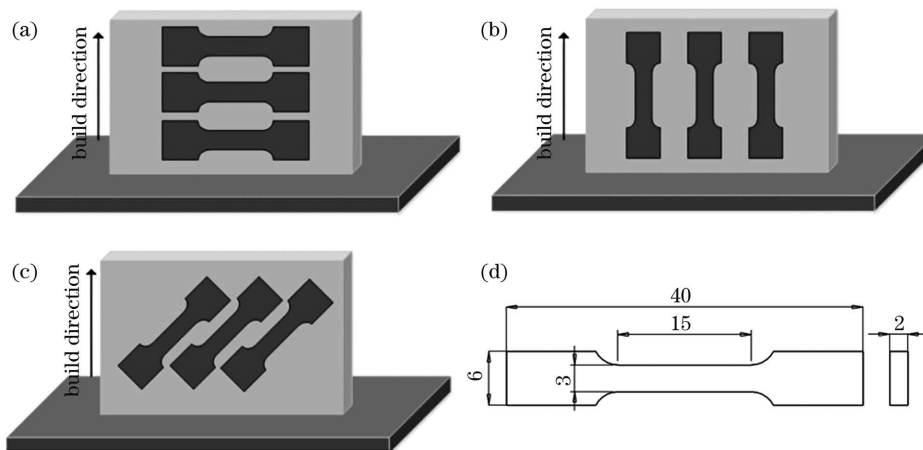


图 3 拉伸样试样的取样方向及尺寸示意图。(a)垂直于构建方向;(b)平行于构建方向;(c)斜 45°方向;(d)拉伸试样的尺寸  
Fig. 3 Specimen orientation and size for tensile test. (a) Perpendicular to build direction; (b) parallel to build direction; (c) 45° inclination; (d) dimension of tensile specimens

采用与拉伸试样相同的工艺参数成型尺寸为 80 mm×3 mm×10 mm 的薄壁件,并在样件中部沿竖直方向取样,以基板与薄壁件结合处中部为起

点,每隔 1 mm 取一点测量显微硬度(测量仪器为 DHV-1000 型显微硬度计),同时采用金相显微镜观察该部位的显微组织。

### 3 试验结果与讨论

#### 3.1 激光/等离子沉积成型单道的特征对比

通过测量沉积前后的基板质量来计算粉末利用

表 4 粉末利用率的测算结果

Table 4 Calculated powder usage ratio

Heat source	Process parameter	$m_0/g$	$m_1/g$	$t/s$	$m_p/g$	$\Phi/\%$	Average $\Phi/\%$
Laser	2000 W, 10 mm·s <sup>-1</sup> , 24 g·min <sup>-1</sup>	1747.5	1748.7	8	3.2	37.5	35.9
	2000 W, 5 mm·s <sup>-1</sup> , 24 g·min <sup>-1</sup>	1748.8	1750.9	16	6.4	32.8	
	2500 W, 10 mm·s <sup>-1</sup> , 24 g·min <sup>-1</sup>	1750.9	1752.1	8	3.2	37.5	
Plasma arc	30 A, 5 mm·s <sup>-1</sup> , 12 g·min <sup>-1</sup>	1747.5	1749.8	16	3.2	71.9	72.9
	40 A, 5 mm·s <sup>-1</sup> , 12 g·min <sup>-1</sup>	1752.0	1754.3	16	3.2	71.9	
	50 A, 5 mm·s <sup>-1</sup> , 12 g·min <sup>-1</sup>	1756.6	1759.0	16	3.2	75.0	

由表 4 可以看出:在同一热源下,不同工艺参数下的粉末利用率较为稳定,激光定向能量沉积的平均粉末利用率为 35.9%,而等离子定向能量沉积的平均粉末利用率可达 72.9%,其粉末利用率是激光定向能量沉积的两倍。这是由于等离子弧是一种高速流体,会对粉末产生轴向加速作用<sup>[12]</sup>,加快粉末进入熔池的速度,而激光定向能量沉积的粉末利用率主要取决于粉末的汇聚效果和光斑大小。

图 4 为等离子和激光定向能量沉积单道的截面形貌。在未预热的情况下,等离子定向能量沉积单道的熔深非常浅,而激光定向能量沉积单道与基板形成

了良好的冶金结合。这是由于激光的功率密度高于等离子弧,前者能迅速熔化甚至气化基板材料,并在金属蒸气压力作用下形成了小孔,其过程类似深熔焊;而本试验中等离子定向能量沉积中的电流很小,属于微束等离子体的范围,等离子弧主要通过融化粉末和基板表层形成熔池,过程类于似热传导焊,熔深较浅。因此,在进行低电流等离子定向能量沉积时,最好先对基板进行预热处理,或在首层使用高于正常工艺的电流,并在后续层逐步将电流降低到正常加工的电流。当使用激光和等离子弧进行复合制造时,首层应使用激光沉积,以保证沉积层与基板的结合质量。

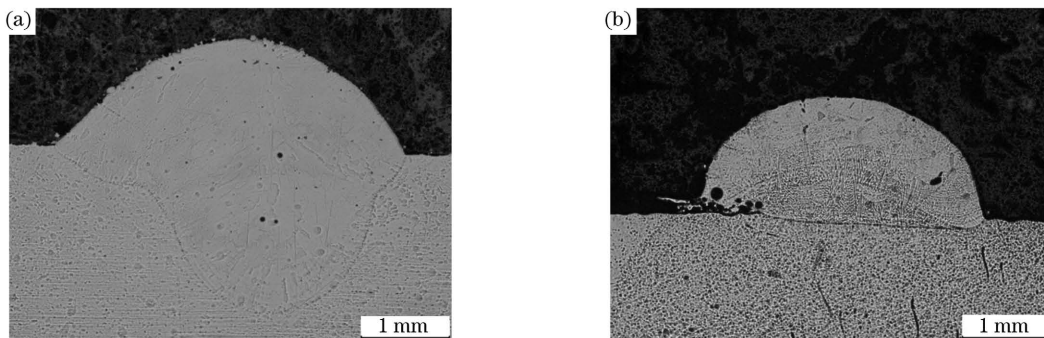


图 4 沉积单道的横截面。(a)激光定向能量沉积;(b)等离子弧定向能量沉积

Fig. 4 Cross-section of deposited single track. (a) Laser directed energy deposition; (b) plasma arc directed energy deposition

#### 3.2 激光/等离子成型薄壁件的尺寸特征对比

表 5 为激光定向能量沉积 316L 不锈钢的二次正交旋转试验结果。使用 Design-Expert 软件对试验数据进行回归统计,分析激光功率、送粉速率、扫描速度以及三者之间的交互关系对成型尺寸的影响。首先先将各因素的一次项、二次项、因素间交互项列入考察范围,进行方差分析;然后根据显著性检验值的大小逐步剔除影响较小的交互项,得出激光定向能量沉积 316L 不锈钢层宽和层高的回归方程。层宽  $W$  的回归方程为

$$W = 18.15 - 0.003173P - 0.041101V - 0.694491F + 1.2 \times 10^{-5}PV + 2.66 \times 10^{-4}PF + 0.00201FV - 6.97917 \times 10^{-7}PFV, \quad (1)$$

层高  $H$  的回归方程为

$$H = -0.560329 + 1.3 \times 10^{-4}P + 0.001111V + 0.069086F - 2.7 \times 10^{-7}PV - 2.9 \times 10^{-6}PF - 6.8 \times 10^{-5}FV, \quad (2)$$

式中: $P$  表示激光功率; $F$  表示送粉速率; $V$  表示激光的扫描速度。激光定向能量沉积 316L 不锈钢尺寸预测模型的方差分析如表 6 所示。

表 5 二次正交旋转试验结果

Table 5 Quadratic regression orthogonal rotation experimental results

No.	Laser power / W	Scanning speed / (mm·min <sup>-1</sup> )	Powder feed rate / (g·min <sup>-1</sup> )	Average width / mm	Average height / mm
1	2500	480	21	6.61	0.65
2	2500	480	10.9	5.17	0.33
3	2500	278	21	8.17	0.87
4	2500	480	21	6.57	0.63
5	3341	480	21	7.09	0.52
6	3000	360	27	8.16	0.92
7	1659	480	21	5.43	0.62
8	2500	480	21	6.06	0.63
9	2500	480	21	6.19	0.61
10	3000	600	27	6.14	0.59
11	2000	600	15	4.21	0.38
12	2000	360	27	6.81	0.95
13	2500	480	31.1	7.52	0.80
14	2500	480	21	6.81	0.51
15	2000	600	27	6.54	0.72
16	3000	360	15	7.42	0.42
17	2500	682	21	5.33	0.34
18	2000	360	15	6.25	0.45
19	2500	480	21	6.36	0.49
20	3000	600	15	5.64	0.32

表 6 激光定向能量沉积 316L 不锈钢尺寸预测模型的方差分析

Table 6 Variance analysis of laser directed energy deposited 316L stainless steel geometry prediction model

Dependent variable	Source	Sum of squares	Degree of freedom	Mean square	F-value	P-value
Layer width	Model	17.82	7	2.55	37.20	<0.0001
	Laser power (A)	1.32	1	1.32	19.28	0.0009
	Scanning speed (B)	8.68	1	8.68	126.80	<0.0001
	Powder feed rate (C)	4.52	1	4.52	66.10	<0.0001
	AB	0.2775	1	0.2775	4.06	0.067
	AC	0.7049	1	0.7049	10.30	0.0075
	BC	0.2926	1	0.2926	4.28	0.0609
	ABC	0.5050	1	0.5050	7.38	0.0187
	Layer height	Model	0.6490	6	0.1082	26.12
Laser power (A)		0.0144	1	0.0144	3.47	0.0852
Scanning speed (B)		0.1925	1	0.1925	46.49	<0.0001
Powder feed rate (C)		0.2194	1	0.2194	52.99	<0.0001
AB		0.0021	1	0.0021	0.5102	0.4877
AC		0.0006	1	0.0006	0.1479	0.7067
BC		0.0190	1	0.0190	4.59	0.0516

层宽模型的  $F$  值为 37.20, 层高模型的  $F$  值为 26.12, 且它们的  $P$  值均小于 0.0001, 表明这两个模

型都是显著的; 层宽模型的拟合优度  $R^2$  为 0.9559, 层高模型的  $R^2$  为 0.9234, 表明这两个模型都较为

合理;层宽模型的信噪比(Adeq precision)为 25.4,层高模型的信噪比为 17.4,表明模型的预测性能较好。由方差分析的结果可知,在激光定向能量沉积薄壁件的主要参数中,扫描速度对层宽的影响最大,然后依次为送粉量和激光功率,送粉量对层高的影响最大,然后依次为扫描速度和激光功率。

关于等离子定向能量沉积 316L 不锈钢的尺寸预测模型,本课题组已进行了相关工作<sup>[13]</sup>,下面直接给出模型及方差分析结果(表 7)。等离子定向能量沉积 316L 不锈钢层宽的回归方程为

$$W = 12.28181 - 0.401244I - 0.009403V + 0.474901F - 1.25 \times 10^{-6}IV + 0.008456IF + 0.000287FV + 0.004883I^2 + 9.41112 \times 10^{-6}V^2 - 0.019429F^2, \quad (3)$$

层高的回归方程为

$$H = 0.812808 + 0.004670I + 9.59 \times 10^{-4}V - 0.149667F - 3.75 \times 10^{-6}IV - 0.001397IF - 1.4 \times 10^{-4}FV + 3.6 \times 10^{-5}I^2 - 1.67 \times 10^{-7}V^2 + 0.018995F^2. \quad (4)$$

表 7 等离子定向能量沉积 316L 不锈钢尺寸预测模型的方差分析

Table 7 Variance analysis of plasma arc directed energy deposited 316L stainless steel geometry prediction model

Dependent variable	Source	Sum of squares	Degree of freedom	Mean square	F-value	P-value
Layer width	Model	16.55	9	1.84	26.84	<0.0001
	Current (A)	4.37	1	4.37	63.75	<0.0001
	Scanning speed (B)	2.43	1	2.43	35.47	0.0001
	Powder feed rate (C)	5.93	1	5.93	86.51	<0.0001
	AB	0	1	0	0.0002	0.9895
	AC	0.1653	1	0.1653	2.41	0.1514
	BC	0.019	1	0.019	0.2774	0.6099
	A <sup>2</sup>	3.44	1	3.44	50.15	<0.0001
	B <sup>2</sup>	0.1276	1	0.1276	1.86	0.2023
	C <sup>2</sup>	0.0454	1	0.0454	0.663	0.4345
Layer height	Model	0.1869	9	0.0208	17.16	<0.0001
	Current (A)	0.0356	1	0.0356	29.39	0.0003
	Scanning speed (B)	0.0268	1	0.0268	22.12	0.0008
	Powder feed rate (C)	0.0712	1	0.0712	58.89	<0.0001
	AB	0.0001	1	0.0001	0.0930	0.7667
	AC	0.0045	1	0.0045	3.73	0.0822
	BC	0.0045	1	0.0045	3.73	0.0822
	A <sup>2</sup>	0.0002	1	0.0002	0.1570	0.7003
	B <sup>2</sup>	0	1	0	0.0334	0.8587
	C <sup>2</sup>	0.0434	1	0.0434	35.90	0.0001

在等离子定向能量沉积薄壁件的主要参数中,电流对层宽的影响最大,之后依次为送粉量、扫描速度,送粉量对层高的影响最大,之后依次为电流、扫描速度。

仅考虑单因素作用时,两种工艺下沉积参数对尺寸的影响趋势是一致的:随着能量输入增加,层宽增加,层高降低;随着送粉量增加,层宽和层高都增加;随着扫描速度增加,层宽和层高都降低。但在各因素交互作用的影响下,两种工艺下的沉积参数对层宽、层高的影响程度不同:在等离子定向能量沉积

过程中,能量输入对层宽和层高的影响占主导地位,扫描速度的影响不及其他两个参数;而在激光定向能量沉积过程中,激光功率的影响不及其他两个参数,扫描速度的影响占主导地位。激光功率参数的 F 值相比其他两个参数的小很多,这可能是由于材料对激光的吸收率较小,实际用于熔化粉末的能量输入比例较小。

### 3.3 激光/等离子定向能量沉积 316L 不锈钢的微观组织和力学性能

图 5 为两种热源定向能量沉积 316L 不锈钢横

截面的显微组织。在定向能量沉积过程中,熔池主要通过基体传热,组织从基体外延生长成柱状晶,但由于两者的能量输入有所不同,柱状晶的尺寸及生长方向存在明显差异。在等离子定向能量沉积试样中,柱状晶的生长方向与沉积方向基本一致,但存在少量转向生长的柱状晶,这些转向柱状晶的形成是由于柱状晶的生长不完全受热流方向控制,但会选择与热流方向最为接近的方向生长<sup>[14]</sup>。等离子定

向能量沉积试样中的柱状晶跨度较长,可达毫米级别,且二次枝晶发达,而激光定向能量沉积试样中的柱状晶较短,生长方向也不一致,熔池边界上的晶粒主要沿垂直于边界方向生长。Zheng 等<sup>[15]</sup>也在激光定向能量沉积过程中观察到了这种复杂的微观凝固组织,并认为熔池内复杂的对流导致柱状晶破碎并重新形核,重新生长的晶体沿着最高温度梯度的方向生长。

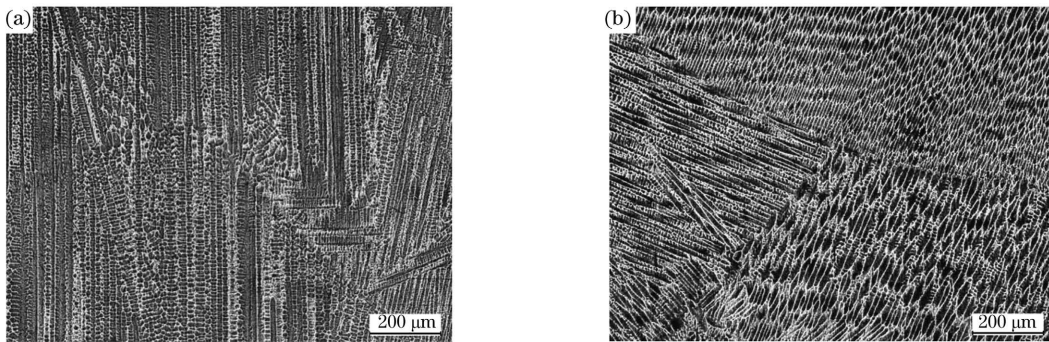


图 5 316L 不锈钢的显微组织。(a)等离子定向能量沉积;(b)激光定向能量沉积

Fig. 5 Microstructures of 316L stainless steel. (a) Plasma arc directed energy deposition; (b) laser directed energy deposition

图 6 为两种热源沉积试样的拉伸试验结果,激光成型和等离子成型试样的抗拉强度(UTS)分别可达 593 MPa 和 570 MPa。两种热源沉积试样的屈服强度(YS)较为接近,并且在不同的构建方向上没有表现出明显的各向异性;与平行于沉积方向相比,垂直于沉积方向取样的拉伸试样具有更高的抗拉强度,斜 45°取样的拉伸试样的抗拉强度介于两者之间。除了平行于沉积方向取样的拉伸试样外,等离子定向能量沉积试样的抗拉强度均低于激光定向能量沉积试样。平行于沉积方向取样的拉伸试样

由于应力直接作用于层间,其拉伸性能受层间结合质量的影响较大,而且层间的氧化、未熔合气孔等缺陷也会导致强度下降。对于垂直于沉积方向取样的拉伸试样,试验力与每层的熔道方向平行,层间缺陷的影响较小。激光定向能量沉积试样中柱状晶的生长方向更为杂乱,晶界的存在阻碍了位错运动;等离子定向能量沉积试样中的柱状晶基本沿着沉积方向生长,仅存在少量转向生长的柱状晶。因此,垂直于沉积方向取样的激光定向能量沉积试样较等离子定向能量沉积试样的抗拉强度更高。

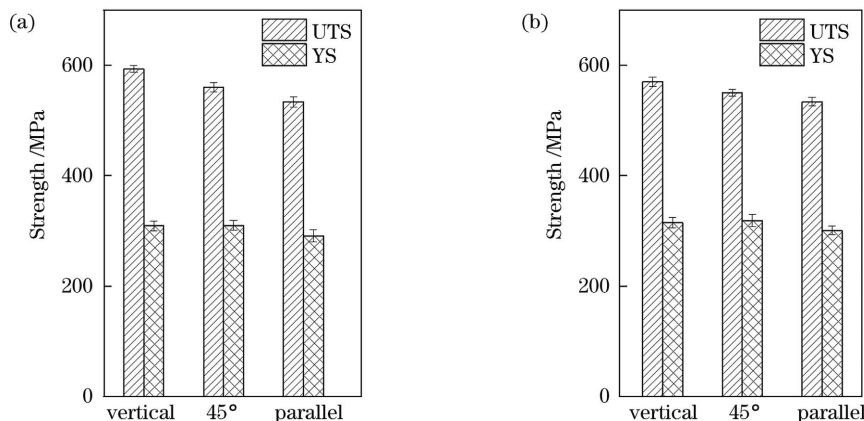


图 6 两种热源沉积试样的拉伸试验结果。(a)激光定向能量沉积;(b)等离子定向能量沉积

Fig. 6 Tensile test results of samples fabricated using two different energy sources. (a) Laser directed energy deposition; (b) plasma arc directed energy deposition

图 7 为两种热源沉积试样横截面上的显微硬度,可见:随着采样距离的增加,两种热源沉积试样

的硬度值均表现出了先降低再升高的趋势。这是因为底层散热较快,冷却速率较大,而中部不仅冷却速

率下降,还会受到后续层加工高温回火的影响,晶粒尺寸有增大的趋势;顶层受高温回火的影响较小,而且与低温的保护气接触,冷却速率有所提高。激光成型试样显微硬度的平均值为 187 HV,等离子成型试样显微硬度的平均值为 191 HV,两者的差距并不大,这与前文所述的两者有相近的屈服强度相对应。

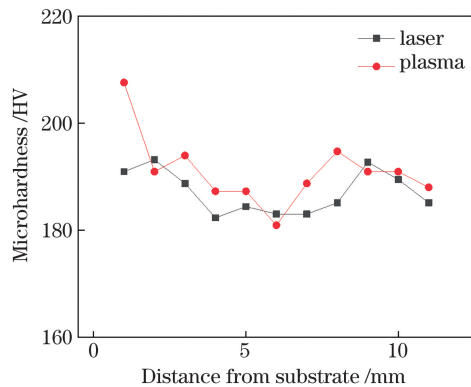


图 7 两种沉积试样的显微硬度

Fig. 7 Microhardness of specimens deposited with two hear sources

## 4 结 论

等离子定向能量沉积的粉末利用率显著高于激光定向能量沉积的粉末利用率,但在未预热的基板上,等离子定向能量沉积首层的稀释率非常低,这可能会导致界面的结合强度不足。

建立了激光沉积 316L 不锈钢薄壁件层宽和层高的预测模型,对比了两种工艺的沉积参数对层高和层宽的影响。代表能量输入的电流对等离子沉积样件的层宽、层高有较大影响,而激光功率对层宽、层高的影响不如送粉量和扫描速度这两个参数。

在小电流和高功率激光条件下,等离子定向能量沉积可成型出性能接近激光定向能量沉积的样件,但两者的显微组织存在较大区别:等离子定向能量沉积试样中的晶粒更趋向于定向生长,柱状晶尺寸较长,而在激光定向能量沉积试样中,不同区域的晶粒生长方向不同,柱状晶尺寸也更小。

## 参 考 文 献

[1] Gibson I, Rosen D, Stucker B. Direct digital manufacturing [M]// Additive manufacturing technologies. New York: Springer, 2015: 375-397.  
 [2] Horn T J, Harrysson O L. Overview of current additive manufacturing technologies and selected applications[J]. Science Progress, 2012, 95(3): 255-282.  
 [3] Rodrigues T A, Duarte V, Miranda R M, et al.

Current status and perspectives on wire and arc additive manufacturing (WAAM) [J]. Materials, 2019, 12(7): E1121.

- [4] Griffith M L, Keicher D M, Atwood C L. Free form fabrication of metallic components using laser engineered net shaping[C]//1996 International Solid Freeform Fabrication Symposium. [S. l.: s. n.], 1996.  
 [5] Sciammarella F, Salehi Najafabadi B. Processing parameter DOE for 316L using directed energy deposition [J]. Journal of Manufacturing and Materials Processing, 2018, 2(3): 61.  
 [6] Yadollahi A, Shamsaei N, Thompson S M, et al. Effects of process time interval and heat treatment on the mechanical and microstructural properties of direct laser deposited 316L stainless steel [J]. Materials Science and Engineering A, 2015, 644: 171-183.  
 [7] Saboori A, Piscopo G, Lai M, et al. An investigation on the effect of deposition pattern on the microstructure, mechanical properties and residual stress of 316L produced by directed energy deposition [J]. Materials Science and Engineering A, 2020, 780: 139179.  
 [8] Chen X H, Li J, Cheng X, et al. Microstructure and mechanical properties of the austenitic stainless steel 316L fabricated by gas metal arc additive manufacturing[J]. Materials Science and Engineering A, 2017, 703: 567-577.  
 [9] Wang K B, Liu Y X, Lü Y H, et al. Influence of processing parameters on microstructure and mechanical property of pulsed plasma arc additive manufactured IN738LC superalloy [J]. Materials Reports, 2021, 35(2): 2086-2091.  
 王凯博, 刘玉欣, 吕耀辉, 等. 工艺参数对脉冲等离子弧增材制造 IN738LC 合金组织与性能的影响[J]. 材料导报, 2021, 35(2): 2086-2091.  
 [10] Guo P, Zou B, Huang C Z, et al. Study on microstructure, mechanical properties and machinability of efficiently additive manufactured AISI 316L stainless steel by high-power direct laser deposition [J]. Journal of Materials Processing Technology, 2017, 240: 12-22.  
 [11] Wang F X, He J P, Xiang F, et al. Study on multi-parameter control system of micro-plasma arc welding [C] // 2010 International Conference on Intelligent System Design and Engineering Application, October 13-14, 2010, Changsha, China. New York: IEEE Press, 2010: 463-466.  
 [12] Wang X B, Zhang W Y. Theoretical evaluation of powders transportation process in plasma transferred-



- arc space [J]. Transactions of the China Welding Institution, 2000, 21(4): 33-37, 99.
- 王惜宝, 张文钺. 等离子弧粉末堆焊过程中粉末颗粒的输运行为[J]. 焊接学报, 2000, 21(4): 33-37, 99.
- [13] Yang Y Q, Weng C W, Zhou Q, et al. Research on the process and prediction model for size of 316L stainless steel fabricated by plasma arc additive manufacturing [J]. Journal of Mechanical Engineering, 2019, 55(15): 31-38.
- 杨永强, 翁昌威, 周权, 等. 316L 不锈钢等离子增材制造工艺与尺寸预测模型研究[J]. 机械工程学报, 2019, 55(15): 31-38.
- [14] Yang S, Huang W D, Liu W J, et al. Research on laser rapid directional solidification with ultra-high temperature gradient[J]. Chinese Journal of Lasers, 2002, 29(5): 475-479.
- 杨森, 黄卫东, 刘文今, 等. 激光超高温梯度快速定向凝固研究[J]. 中国激光, 2002, 29(5): 475-479.
- [15] Zheng B, Haley J C, Yang N, et al. On the evolution of microstructure and defect control in 316L SS components fabricated via directed energy deposition [J]. Materials Science and Engineering A, 2019, 764: 138243.

## Comparative Forming Size and Mechanical Properties of 316L Stainless Steel Fabricated Using Laser /Plasma Arc Directed Energy Deposition

Qin Wentao, Yang Yongqiang<sup>\*</sup>, Weng Changwei, Han Changjun

*School of Mechanical and Automotive Engineering, South China University of Technology, Guangzhou, Guangdong 510640, China*

### Abstract

**Objective** Directed energy deposition (DED) is a popular additive manufacturing technology that uses a high-energy beam to melt metal powders and deposit them onto a substrate. It has the advantage of printing large-scale metal parts efficiently. Common high-energy sources for DED systems include laser, plasma arc, and electron beam. Laser DED (L-DED) is considered to print parts with better mechanical performance but low printing efficiency compared to plasma arc DED (PA-DED). Furthermore, there is a significant difference in the metallurgical mechanism between the two processes. In this study, we compared the geometry, microstructure, and mechanical properties of 316L stainless steel deposited by L-DED and PA-DED processes. The underlying mechanisms of the difference in geometry, microstructure, and mechanical properties of samples printed by the two processes were discussed.

**Methods** An in-house developed DED system that consists of a fiber laser with a maximum power of 6 kW, two robot arms, one L-DED module, and one PA-DED module was used. A 316L stainless steel powder with a particle size ranging from 60 to 125  $\mu\text{m}$  was adopted as the feedstock for the two printing processes. Single tracks with a length of 80 mm were printed via the two processes, and their cross-sections were etched for geometry measurement. A quadratic regression orthogonal experiment was designed to investigate the effect of energy input, scanning velocity, and powder feeding velocity on the geometry of printed thin walls. The dimensions of the thin walls are 80 mm  $\times$  3 mm  $\times$  100 mm. The average layer width and height were measured from the middle location of the thin walls. The L-DED process parameters included a laser power of 2000 W, a scanning speed of 10 mm/s, and a powder feed rate of 24 g/min. The PA-DED process parameters included a current of 30 A, a scanning speed of 5 mm/s, and a powder feed rate of 12 g/min. Samples perpendicular to the build direction, parallel to the build direction, and inclined at 45° were machined for tensile testing. Microstructures of the printed thin walls were also observed from their cross-section locations.

**Results and Discussions** The average powder utilization rate of the two printing processes was calculated by measuring the weight difference before and after the deposition (Table 4). The average powder utilization rates of L-DED and PA-DED were 35.9% and 72.9%, respectively. The twice powder utilization rate of PA-DED compared with L-DED was attributed to the high-velocity of plasma arc that could accelerate powder particles deposited into melt pools during printing. The cross-sectional morphologies of the single tracks indicated that L-DED enabled a better metallurgical bonding between the melt pool and substrate than the PA-DED process. This was ascribed to the higher energy density of L-DED, increasing the penetration of the melt pool. The entire process was similar to deep

penetration welding. In contrast, the small current used in PA-DED led to slight melting of the substrate surface, where the process was similar to conduction welding with a shallow melt pool. Therefore, a preheating process for the substrate or the utilization of a high current for the first printing layer should be conducted in the PA-DED process to enhance the bonding. The regression equations of layer width and height for PA-DED and L-DED were realized. The variance analysis of orthogonal experimental results (Tables 6 and 7) indicated that the process parameters of PA-DED and L-DED exhibited different influence orders on layer geometry. In the PA-DED process, the process parameters that influenced the layer width by the descending order were current, powder feed rate, and scanning speed, whereas the parameters that influenced the layer height by the descending order were powder feed rate, current, and scanning speed. Comparatively, in L-DED, the process parameters that influenced the layer width by the descending order were scanning speed, powder feed rate, and laser power, whereas the parameters that influenced the layer height by the descending order were powder feed rate, scanning speed, and laser power. The influence trend of process parameters on the geometry of the two processes was consistent when only a single factor was considered. As the energy input increased, the floor width increased and the floor height decreased; the layer width and height increased with an increase in the powder feeding quantity and decreased with an increase in the scanning speed. The microstructure morphologies (Fig. 5) of samples printed by the two processes were slightly different. PA-DED samples were dominated by directional growth long columnar grains with sizes up to millimeters, and many secondary dendrites could be obtained. However, L-DED samples showed shorter columnar grains and various growth directions in different regions. Particularly, the grains grew mainly perpendicular to the melt pool boundary. Tensile and microhardness testing results (Fig.6 and Fig.7) showed that samples fabricated by PA-DED achieved comparable mechanical properties to those printed by L-DED. The tensile strength of the samples was 593 and 570 MPa for L-DED and PA-DED, respectively.

**Conclusions** The powder utilization rate of PA-DED was significantly higher than that of L-DED. However, the dilution rate of the first layer of PA-DED was low on the substrate without preheating, leading to insufficient interfacial bonding strength. The prediction equations of the layer width and height of 316L thin-walled parts by L-DED were established. The effects of process parameters on the geometry of the two printing processes were compared. Current had a great influence on the layer width and height during PA-DED, whereas the influence of laser power on the layer width and height during L-DED could not be compared with the powder feed rate and scanning speed. The microstructure of PA-DED samples tended to grow directionally and their columnar grains were longer. L-DED samples obtained smaller columnar grains, which possessed various growth directions in different regions.

**Key words** laser technique; directed energy deposition; laser additive manufacturing; plasma arc additive manufacturing; 316L stainless steel

**OCIS codes** 350.3390; 350.3850; 350.5400